ELSEVIER

Journal of Fluids and Structures 23 (2007) 1189–1206

JOURNAL OF FLUIDS AND STRUCTURES

www.elsevier.com/locate/jfs

Turbulent wake and vortex shedding for a stack partially immersed in a turbulent boundary layer

M.S. Adaramola[a], D. Sumner[b,*], D.J. Bergstrom[b]

[a]*Division of Environmental Engineering, University of Saskatchewan, 57 Campus Drive, Saskatoon, Sask., Canada S7N 5A9*
[b]*Department of Mechanical Engineering, University of Saskatchewan, 57 Campus Drive, Saskatoon, Sask., Canada S7N 5A9*

Received 24 August 2006; accepted 5 May 2007
Available online 10 July 2007

Abstract

The effect of the jet-to-cross-flow velocity ratio, R, on the turbulent wake and Kármán vortex shedding for a cylindrical stack of aspect ratio AR = 9 was investigated in a low-speed wind tunnel using thermal anemometry. The cross-flow Reynolds number was $\mathrm{Re}_D = 2.3 \times 10^4$, the jet Reynolds number ranged from $\mathrm{Re}_d = 7.6 \times 10^3$ to 4.7×10^4, and R was varied from 0 to 3. The stack was partially immersed in a flat-plate turbulent boundary layer, with a boundary layer thickness-to-stack-height ratio of $\delta/H = 0.5$ at the location of the stack. From the behaviour of the turbulent wake and the vortex shedding, the flow around the stack could be classified into three regimes depending on the value of R, which were the downwash ($R < 0.7$), cross-wind-dominated ($0.7 \leqslant R < 1.5$), and jet-dominated ($R \geqslant 1.5$) flow regimes. Each flow regime had a distinct structure to the mean velocity (streamwise and wall-normal directions), turbulence intensity (streamwise and wall-normal directions), and Reynolds shear stress fields, as well as the variation of the Strouhal number and the power spectrum along the stack height.

1. Introduction

Stacks are used to reduce the ground-level concentration of an exhaust gas by emission of the exhaust gas at greater heights. For a stack mounted on a building rooftop, the local velocity field, the origin and development of the rooftop boundary layer, the proximity of other buildings and structures, the stack exit temperature and velocity, and the wind velocity and direction, are major factors that affect the rise and dispersion of the stack jet or plume (Wilson, 1979; Schulman and Scire, 1991). Engineering design guidelines for rooftop-mounted stacks are well established (ASHRAE, 1999, 2001) and the behaviour of stack jets and buoyant plumes has been extensively studied (Briggs, 1984).

In addition to the behaviour of the jet or plume, many of the same factors mentioned above also influence the local flow field of the stack itself. In order to understand the local flow field around a rooftop stack, which has not been extensively reported in the literature, there is need to study the jet and its interaction with near field of the stack. In the present study, the turbulent wake of a short cylindrical stack is investigated experimentally in a low-speed wind tunnel, to provide more insight into the near-field behaviour of the flow under different jet flow conditions. In addition, the effects of the jet on Kármán vortex shedding from the stack are also examined.

*Corresponding author. Tel.: +1 306 966 5537; fax: +1 306 966 5427.
E-mail address: david.sumner@usask.ca (D. Sumner).

0889-9746/$ - see front matter
doi:10.1016/j.jfluidstructs.2007.05.001

2. Background

The local flow field of a stack involves three fundamental yet complex flows: the plane wall boundary layer flow on the ground plane, the separated flow field and wake of a finite circular cylinder (representing the simplest possible stack geometry), and the development of an elevated round jet in cross-flow (representing the exhaust jet exiting the stack). The flow field of a stack of uniform cylindrical shape, with external diameter, D, internal diameter, d, and height, H, is shown schematically in Fig. 1. In Fig. 1(b), the stack is shown partially immersed in a turbulent flat-plate boundary layer on the ground plane, with freestream velocity, U_∞, boundary layer mean velocity profile, $\bar{U}(z)$ (where z is the wall-normal coordinate), and boundary layer thickness, δ. Also identified in Fig. 1(b) are the stack and jet wakes, as well as the rise, $h(x)$ (where x is the streamwise coordinate), of the elevated turbulent jet after it exits the stack (where U_e is the average jet exit velocity).

The flow around the stack and along its height is influenced by the stack Reynolds number, $\mathrm{Re}_D = \rho_\infty U_\infty D/\mu_\infty$ (where ρ_∞ and μ_∞ are the density and dynamic viscosity of the approach flow, respectively), the stack aspect ratio, $\mathrm{AR} = H/D$, and the relative thickness of the flat-plate boundary layer at the location of the stack, δ/H. The behaviour of the round jet exiting the stack is governed by the jet Reynolds number, $\mathrm{Re}_d = \rho_e U_e d/\mu_e$ (where ρ_e and μ_e are the density and dynamic viscosity of the jet, respectively). If the jet is nonbuoyant, $\rho_\infty = \rho_e$ and $\mu_\infty = \mu_e$, and its interaction with the cross-flow is influenced primarily by the jet-to-cross-flow velocity ratio, $R = U_e/U_\infty$ and to a lesser extent by the diameter ratio, d/D. For buoyant jets (or plumes), the main parameter of influence is the momentum flux ratio, $R_m = (\rho_e U_e^2)/(\rho_\infty U_\infty^2)$.

2.1. Flow around a finite circular cylinder

The simplest stack geometry can be represented by a uniform circular cylinder of finite height mounted normal to a plane wall or ground plane. Flow around the base of the cylinder and over the free end causes the flow field to become

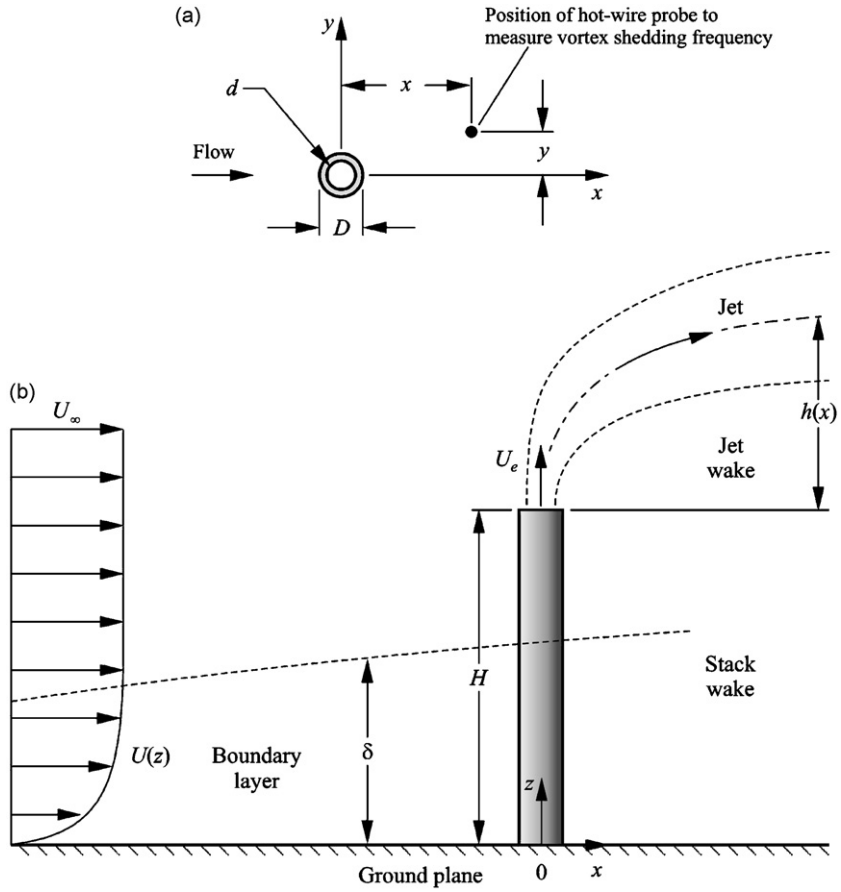

Fig. 1. Stack of uniform circular cross-section mounted normal to a ground plane and partially immersed in a turbulent flat-plate boundary layer: (a) top view; (b) side view.

strongly three dimensional. Compared to the "infinite" (2-D) cylinder, there are marked changes in the near-wake flow structure, including the vortex formation region, vortex shedding behaviour, and surface pressure distribution. There are also distinct flow pattern changes along the cylinder height from the free end to the base. In the base region, which is immersed in the flat-plate boundary layer, the fluid recirculates at the leading edge of the cylinder. The fluid is then swept around the cylinder base, rotating and rolling up into a horseshoe vortex. Near the free end, the shear layer from the free end separates and interacts with the two shear layers that separate from the sides of the cylinder. This leads to a pair of counter-rotating tip vortices forming at the free end that extends into the wake (Okamoto and Yagita, 1973; Etzold and Fiedler, 1976; Kawamura et al., 1984; Johnston and Wilson, 1997; Tanaka and Murata, 1999; Sumner et al., 2004). A second pair of vortices, known as the base vortex structures, may be found within the flat-plate boundary layer (Tanaka and Murata, 1999; Sumner et al., 2004). Whether the tip and base vortices are distinct vortex structures themselves, or in fact are Kármán vortex structures with oblique axes (Etzold and Fiedler, 1976) that have undergone stretching or bending near the free end and ground plane (Okamoto and Yagita, 1973; Johnston and Wilson, 1997; Tanaka and Murata, 1999), remains to be clarified.

Only a few studies of the finite circular cylinder have extensively measured the wake velocity field: for example, the time-averaged rotating yaw probe measurements of Tanaka and Murata (1999), the time-averaged LDA measurements of Leder (2003) for a cylinder of AR = 2, the time-averaged PIV measurements of Park and Lee (2004), the time-averaged seven-hole probe measurements of Sumner et al. (2004), and the time-averaged two-component thermal anemometry measurements of Adaramola et al. (2006).

With respect to Kármán vortex shedding from a finite circular cylinder, it is strongly influenced by the tip vortices and a downward-directed local velocity field near the free end referred to as "downwash." The interaction between downwash and Kármán vortex shedding is strongly influenced by AR and δ/H. A general observation in many studies is that the dimensionless vortex shedding frequency, or Strouhal number, St ($= f_s D/U_\infty$, where f_s is the vortex shedding frequency), decreases as AR decreases, because of the increasing influence of downwash. Similarly, the base vortex structures are responsible for an "upwash" flow within the flat-plate boundary layer (Sumner et al., 2004).

For finite circular cylinders of high aspect ratio, St may vary in a cellular fashion along the cylinder height, each cell having a different frequency for uniform flow [e.g., Fox and Apelt (1993)] and for shear flow [e.g., Maull and Young (1973) and Griffin (1985)], with shedding being suppressed near the free end and the base. The number of cells along the cylinder height depends, among other factors, on AR. For AR > 7, more than two cells have been observed [e.g., Fox and Apelt (1993)], while the cellular structure disappears at lower aspect ratios, becoming a single cell of uniform frequency along the entire height for AR < 7 (Uematsu et al., 1990; Okamoto and Sunabashiri, 1992), particularly when δ/H is large (Sakamoto and Oiwake, 1984; Sumner et al., 2004). Below a critical aspect ratio (varying between AR = 1 and 7, depending on δ/H), the flow around the free end may completely suppress antisymmetric Kármán vortex shedding from the cylinder. The cylinder then has a distinct wake structure (Sumner et al., 2004; Adaramola et al., 2006), and symmetric arch vortex shedding may occur (Taniguchi et al., 1981; Okamoto and Sunabashiri, 1992; Lee, 1997; Tanaka and Murata, 1999).

For cylindrical stacks of sufficiently high aspect ratio, the wake structure should change as the influence of downwash lessens with increasing jet-to-cross-flow velocity ratio, R. Kármán vortex shedding then should be expected to occur along most of the stack height, possibly in a cellular fashion. The more complex vortex shedding behaviour of the finite cylinder (compared to the "infinite" cylinder case) is an important consideration when assessing a stack's tendency towards flow-induced vibration (Kitagawa et al., 1997).

2.2. Elevated jet in cross-flow

The behaviour of a turbulent round jet issuing normally into a cross-flow depends on how the jet is injected. The jet can be injected through either an orifice on the ground plane, which is referred to as ground-level source jet, or from an elevated source, as in the case of the stack. There is extensive work on the ground-level source jet in the literature [e.g., McMahon et al. (1971), Andreopoulos and Rodi (1984), Fric and Roshko (1994)]. For the elevated jet in cross-flow, considerable attention in the literature has focused on the jet rise [e.g., Overcamp and Ku (1988)] with relatively fewer studies centred on the local flow field of the stack and jet. These studies have shown the flow field to be characterized by the complex interactions between the jet and stack wake regions, shear produced by the upward momentum of the jet, and downwash (Moussa et al., 1977; Eiff et al., 1995; Eiff and Keffer, 1997, 1999; Huang and Hsieh, 2002, 2003; Huang and Lan, 2005).

From studies of the flow topology in the vertical plane along the wake centreline (the x–z plane, see Fig. 1(b)), Huang and Hsieh (2002, 2003) classified the stack and jet wake flow patterns into four regimes based on the approximate value of R: (i) downwash flow ($R < 0.95$), (ii) cross-wind-dominated flow ($0.95 < R < 1.4$), (iii) transitional flow ($1.4 < R < 2.4$), and (iv) jet-dominated flow ($R > 2.4$). The classification was made for a stack of AR = 25 and $d/D = 0.78$ operating at

$Re_D = 2 \times 10^3$ and $Re_d = 200$ to 8×10^3. The effect of Re_D, Re_d, AR, δ/H and other parameters on the number of flow regimes and the flow regime boundaries has not been extensively studied, however.

In the downwash flow regime, the jet is deflected through a large angle from the vertical axis of the stack. In the cross-wind-dominated flow regime, the downwash effects are reduced in the jet wake. A clockwise vortex forms near the free end of the stack due to interaction between the jet shear and downwash (Huang and Hsieh, 2002, 2003). At higher jet-to-cross-flow velocity ratios, the upward momentum of the jet overcomes the downwash effect, and the jet rises and bends into the freestream. For the jet-dominated flow regime, the high upward momentum of the jet, and the shear produced by the jet, result in a strong upwash velocity field, particularly in the jet wake region (Huang and Hsieh, 2002, 2003; Hsieh and Huang, 2003).

The elevated jet in cross-flow, and the local flow field near the jet exit, were also studied by Eiff et al. (1995) and Eiff and Keffer (1997, 1999). Using spectral analysis, pattern recognition techniques and multipoint hot-wire measurements, they investigated the interaction between the jet and stack wakes at $x/D = 11$ for AR = 6, 8 and 11, $d/D = 0.42$, 0.63, and 0.83, $Re_D = 7.5 \times 10^3$–6.0×10^4, $Re_d = 3.8 \times 10^4$, and $R = 1.5$, 3, and 6. Their studies showed that Kármán-like vortex structures in the stack wake region are "locked-in" to, or synchronized with, similar vortex structures in the jet wake region over a range of velocity ratios ($R = 1.5$, 3 and 6) and diameter ratios ($0.63 \leqslant d/D \leqslant 0.83$). Lock-in does not occur at smaller d/D, however; rather, the vortex dynamics in the jet wake become similar to the ground-level source jet (Eiff and Keffer, 1999). A similar result was also reported by Moussa et al. (1977) for a stack of AR = 24 and $d/D = 0.93$. A comprehensive study of the shear-layer vortices in the stack jet and wake regions, and the dominant frequencies associated with these structures, has been conducted by Huang and Lan (2005).

3. Experimental approach

The present experiments were conducted in a low-speed, closed-return wind tunnel with a test-section of 0.91 m (height) × 1.13 m (width) × 1.96 m (length). The longitudinal freestream turbulence intensity was less than 0.6% and the velocity nonuniformity outside the test section wall boundary layers was less than 0.5%. The test-section floor was fitted with a ground plane. A rough strip located about 200 mm from leading edge of the ground plane was used to produce a turbulent boundary layer at the location of the stack. The experimental set-up for the study is shown schematically in Fig. 2, and was similar to those adopted by Sumner et al. (2004) and Adaramola et al. (2006).

3.1. Experimental apparatus

A cylindrical stack of $H = 171.5$ mm, $D = 19.1$ mm, $d/D = 0.67$, and AR = 9, was used in the present study. The stack was located 700 mm downstream of the rough strip on the ground plane (Fig. 2). The experiments were conducted at a single stack Reynolds number of $Re_D = 2.3 \times 10^4$.

A pair of screens was installed at the stack supply inlet to ensure the flow exiting the stack was turbulent. The exhaust velocity of the nonbuoyant stack jet was varied with two MKS 1559A-200L mass flow controllers arranged in parallel. The jet-to-cross-flow velocity ratio was varied from $R = 0$ (no jet exiting the stack) to $R = 3$, corresponding to momentum flux ratios of $R_m = 0$–9. The jet Reynolds number for the minimum exit velocity, when $R = 0.5$, was

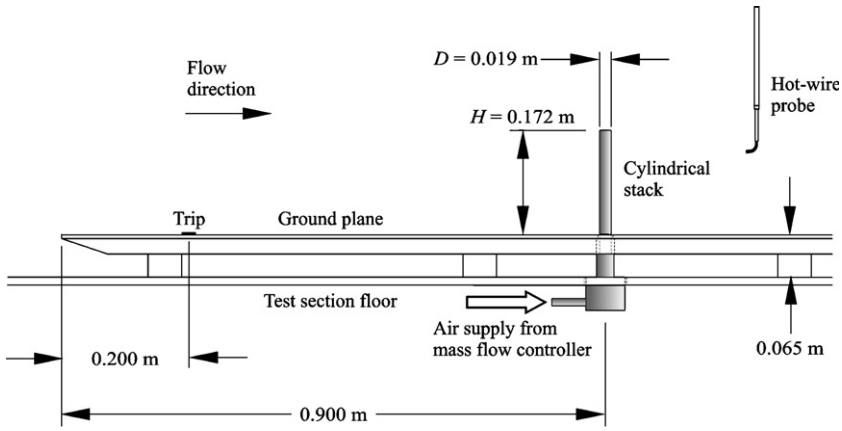

Fig. 2. Schematic of the experimental set-up in the wind tunnel.

$Re_d = 7.6 \times 10^3$ (based on the internal diameter of the stack and the average jet exit velocity). The jet Reynolds number for the maximum exit velocity, when $R = 3$, was $Re_d = 4.7 \times 10^4$.

The mean axial velocity ($\bar{U}_z/U_c$, where U_c is the mean axial centreline velocity) profiles measured at a distance of 12.7 mm (1*d*) from the stack exit at different jet Reynolds numbers are presented in Fig. 3. Few studies of scale-model stacks in the literature report this information. These measurements were made with the X-probe and hot-wire anemometry system described in Section 3.2. The top-hat profiles observed in Fig. 3 are similar to the typical velocity profile for a turbulent pipe flow (Arya and Lape, 1990). At low flow rates, the increase in the mean axial velocity at the outer edges of the jet, as shown in Fig. 3, was attributed to aerodynamic interference between the measuring probe and the stack. Otherwise, there is no significant Reynolds number effect on these profiles. This may be because all the Reynolds numbers considered are in the turbulent flow range and far above the critical Reynolds number for pipe flow.

3.2. Measurement instrumentation

The wind tunnel data were acquired with a computer with a 1.8-GHz Intel Pentium 4 processor, a National Instruments PCI-6031E 16-bit data acquisition board, and LabVIEW software. The freestream conditions were obtained with a Pitot-static probe (United Sensor, 3.2-mm diameter), Datametrics Barocell absolute and differential pressure transducers, and an Analog Devices AD590 integrated circuit temperature transducer.

Wake velocity measurements were made with a TSI model 1243-20 boundary layer X-probe and a TSI IFA-100 constant-temperature anemometer. The X-probe was oriented to measure the streamwise, u, and wall-normal, w, velocity components. The probe was manoeuvred to the measuring points using the wind tunnel's three-axis computer-controlled traversing system. At each measurement point, 100,000 instantaneous velocity data per channel were acquired at a sampling rate of 10 kHz per channel after low-pass filtering at 5 kHz. The probe was calibrated in the freestream using a Pitot-static probe and an automated variable-angle calibrator. Two-dimensional third-order polynomials were fitted to the voltage data to give response equations for the velocity magnitude and the yaw angle. The uncertainties in the streamwise and wall-normal fluctuating velocity components were estimated to be $\pm 4\%$ and $\pm 7\%$, respectively, while the uncertainty in the Reynolds shear stress was estimated to be $\pm 9\%$. For a given value of the velocity ratio, R, the wake velocity field in the cross-stream (y–z) plane was measured over a 5-mm uniform grid at $x/D = 10$. The measurement plane extended in the cross-stream to $y/D = \pm 4$ and to $z/D = 14$ in the wall-normal direction.

The mean streamwise velocity profile of the turbulent boundary layer on the ground plane, at the location of the stack (with the stack removed), is shown in Fig. 4. The boundary layer thickness, δ, was defined as the point where the local mean velocity was 99% of the freestream velocity. At the location of the stack, the boundary layer thickness was $\delta = 83$ mm, the boundary layer shape factor was 1.3, and the Reynolds number based on momentum thickness, θ, was $Re_\theta = 8 \times 10^3$. This boundary layer provided a thickness-to-height ratio of $\delta/H \approx 0.5$.

The vortex formation length, L_f, was determined by measuring the streamwise turbulence intensity profile along the wake centreline at the mid-height of the stack ($z/H = 0.5$). The vortex formation length was defined as the location of the local maximum value of the streamwise turbulence intensity on the wake centreline.

Measurements of the vortex shedding frequency were made with a single-component hot-wire probe (TSI model 1210-T1.5). The probe was located at a fixed streamwise and cross-stream position, $x/D = 3$ and $y/D = 1.5$ (Fig. 1(a)),

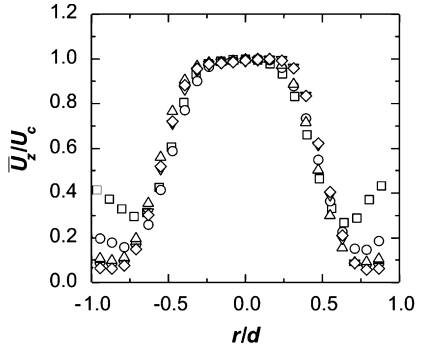

Fig. 3. Mean axial velocity of the stack jet measured at one exit diameter downstream (no wind tunnel cross-flow): □, $Re_d = 7.6 \times 10^3$ (corresponds to $R = 0.5$); ○, $Re_d = 1.5 \times 10^4$ (corresponds to $R = 1$); △, $Re_d = 2.3 \times 10^4$ (corresponds to $R = 1.5$); ▽, $Re_d = 3.0 \times 10^4$ (corresponds to $R = 2$); ◇, $Re_d = 4.7 \times 10^4$ (corresponds to $R = 3$).

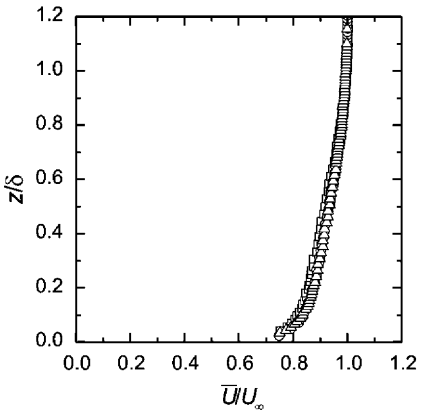

Fig. 4. Mean streamwise velocity profile of the turbulent flat-plate boundary layer on the wind tunnel ground plane: □, $x/D = -10$; ○, $x/D = 0$; △, $x/D = 10$.

with the wall-normal position, z/H, allowed to vary (where $z/H = 0$ corresponds to the wall, $z/H = \delta/H = 0.5$ corresponds to the wall boundary layer thickness at the location of the stack, and $z/H = 1$ corresponds to the height of the stack).

4. Vortex shedding

4.1. Strouhal number and vortex formation length at mid-height ($z/H = 0.5$)

The Strouhal number data measured in the wake at the mid-height of the stack (corresponding to $z/H = 0.5$) are summarized in Table 1 and Fig. 5(a) for various values of R. The result for no flow from the stack ($R = 0$) compares favourably with the finite circular cylinder result of Sumner et al. (2004), which also involved a thick boundary layer on the ground plane ($\delta/H = 0.3$). The Strouhal number measured by Okamoto and Yagita (1973) is higher, but this was for the case of a very thin flat-plate boundary layer ($\delta/H = 0.02$). The results for $R = 1.5$ and 3 compare favourably with the data from Eiff and Keffer (1999).

The trend in the Strouhal number data at mid-height, in Fig. 5(a), shows a gradual increase with velocity ratio, with the Strouhal number approaching the value of an "infinite" cylinder ($\mathrm{St} \approx 0.2$) with an increase in R. There is a more abrupt increase in St at $R \approx 0.7$, which could indicate a change in the stack wake flow regime. The overall effect of the jet-to-cross-flow velocity ratio is to make the stack behave similarly to a finite circular cylinder of higher aspect ratio (which, for sufficiently high aspect ratio, attains the Strouhal number value of an infinite cylinder (Farivar, 1981; Lee and Wang, 1987)); a similar result was noted by Eiff et al. (1995).

The data in Table 1 and Fig. 5(a) also suggest three different types of behaviours for the Strouhal number, with a common low value of St obtained for $R = 0$, 0.5, and 0.6; an elevated intermediate value of St obtained for $R = 0.7$ and 1; and a higher common value of St for $R = 1.5$, 2, 2.5, and 3. 2. From Fig. 5(a) and Table 1, it is seen that the Strouhal number for $R = 3$ ($\mathrm{St} = 0.192$) is slightly lower than when $R = 2.5$ ($\mathrm{St} = 0.195$), but is similar to the data of Eiff and Keffer (1999) for $R = 3$ and $\mathrm{AR} = 8$ ($\mathrm{St} = 0.191$). These small differences may be partially attributed to the measurement uncertainty of the St data, which is conservatively estimated to be about $\pm 1\%$.

Fig. 5(b) shows the vortex formation length, L_f, of the stack measured at mid-height ($z/H = 0.5$) for different jet-to-cross-flow velocity ratios. For an "infinite" circular cylinder, the vortex formation length at $\mathrm{Re}_D = 2.7 \times 10^4$ ranges from $L_f/D = 1.3$ to 1.5, depending on the freestream turbulence intensity (Norberg, 1986; Noca et al., 1998). For a finite circular cylinder, the vortex formation length at mid-height is greater than that of an "infinite" cylinder and is a function of AR and δ/H, obtaining a value of $L_f/D = 3.6$ in the present study for $\delta/H = 0.5$, $L_f/D = 4.4$ in Sumner et al. (2004) for $\delta/H = 0.3$, and $L_f/D = 3.8$ in Park and Lee (2000) for $\delta/H = 0.01$ and $\mathrm{AR} = 10$. As shown in Fig. 5(b), the vortex formation length of the stack decreases as the jet-to-cross-flow velocity ratio increases, and approaches the value for the "infinite" cylinder at high velocity ratios. The reduction in vortex formation length with increasing R is consistent with the behaviour of the Strouhal number at mid-height, as described above and shown in Fig. 5(a), where the jet acts as a bluff body and increases the effective aspect ratio of the stack.

Table 1
Selected Strouhal number data measured at mid-height ($z/H = 0.5$) for a finite circular cylinder or stack of AR = 9 (unless otherwise indicated)

	Re	δ/H	δ/D	St
Okamoto and Yagita (1973), $R = 0$	1.3×10^4	0.02	0.15	0.18
Sumner et al. (2004), $R = 0$	6.0×10^4	0.3	2.6	0.16
$R = 0$	2.3×10^4	0.5	4.6	0.167
$R = 0.5$	2.3×10^4	0.5	4.6	0.169
$R = 0.6$	2.3×10^4	0.5	4.6	0.176
$R = 0.7$	2.3×10^4	0.5	4.6	0.185
$R = 1$	2.3×10^4	0.5	4.6	0.185
$R = 1.5$	2.3×10^4	0.5	4.6	0.190
Eiff and Keffer (1999), $R = 1.5$, AR = 8	4.0×10^4			0.190
$R = 2$	2.3×10^4	0.5	4.6	0.193
$R = 2.5$	2.3×10^4	0.5	4.6	0.195
$R = 3$	2.3×10^4	0.5	4.6	0.192
Eiff and Keffer (1999), $R = 3$, AR = 8	2.2×10^4			0.191
Eiff and Keffer (1999), $R = 6$, AR = 8	1.0×10^4			0.203

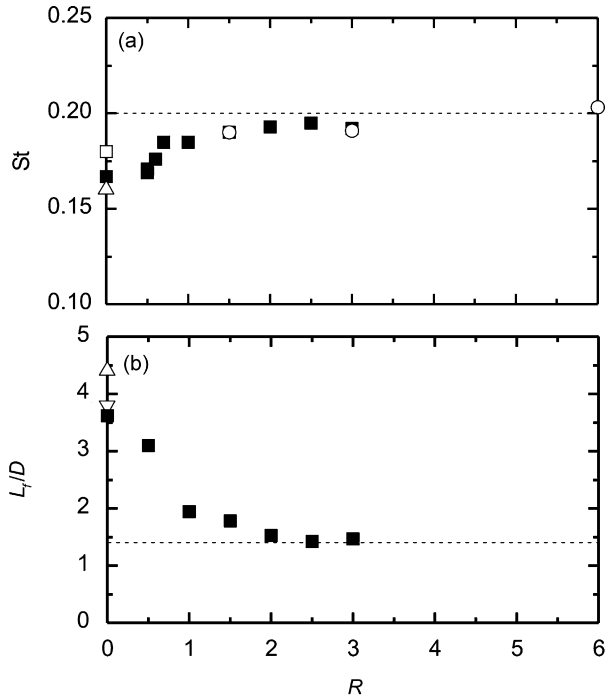

Fig. 5. Measurements at the mid-height position ($z/H = 0.5$) of the stack: (a) Strouhal number, hot-wire probe positioned at $x/D = 3$ and $y/D = 1.5$; (b) vortex formation length. Stack data: ■, current study; ○, Eiff and Keffer (1999), AR = 8, $\mathrm{Re}_D = 2.2 \times 10^4$, δ/H not given. Finite circular cylinder data: □, Okamoto and Yagita (1973), AR = 9, $\mathrm{Re}_D = 1.3 \times 10^4$, $\delta/H = 0.02$; △, Sumner et al. (2004), AR = 9, $\mathrm{Re}_D = 6 \times 10^4$, $\delta/H = 0.3$; ▽, Park and Lee (2000), AR = 10, $\mathrm{Re}_D = 2 \times 10^4$, $\delta/H = 0.01$. Dashed line shows the "infinite" cylinder value.

4.2. Strouhal number variation with height

The variation of the Strouhal number with the height of the stack, z/H, for various jet-to-cross-flow velocity ratios, R, is shown in Fig. 6. Three different types of Strouhal number behaviours were observed. At a low jet-to-cross-flow

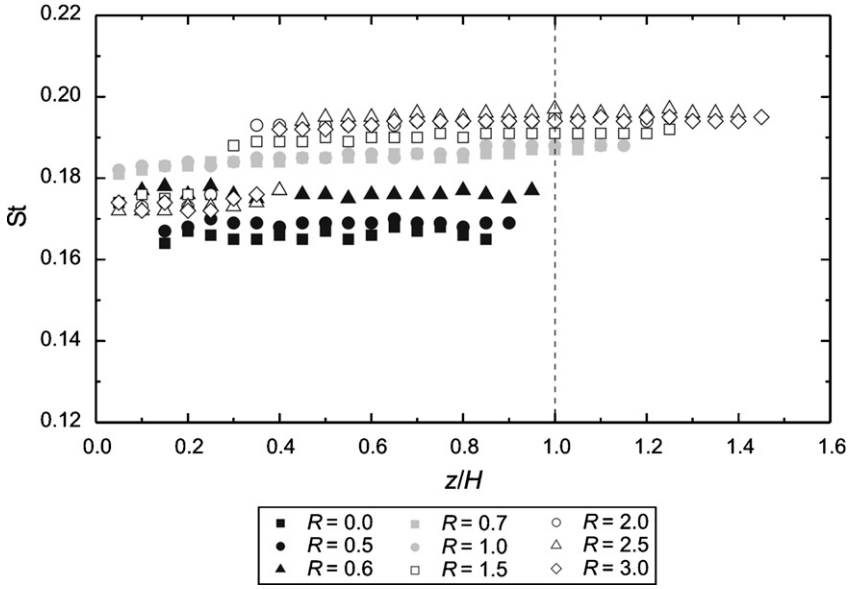

Fig. 6. Strouhal number measured along the height of the stack (the dashed line at $z/H = 1.0$ indicates the top of the stack); the hot-wire probe was positioned at a fixed streamwise and cross-stream location, corresponding to $x/D = 3$ and $y/D = 1.5$, with only the wall-normal position, z/H, allowed to vary).

velocity ratio of $R = 0.5$, the Strouhal number is nearly the same value as that for no jet flow ($R = 0$, or the finite cylinder case). Along the height of the stack, the same Strouhal number value is measured, and no cellular variation of St is observed. Similar behaviour is observed for $R = 0.6$, although the magnitude of the Strouhal number is slightly higher. This uniform shedding along the height corresponds to "one-cell antisymmetric shedding" behaviour (Lee, 1997) and is consistent with the finite-cylinder results for AR = 9 obtained by Sumner et al. (2004). The results from the present study, where $\delta/H = 0.5$, further support the view that a larger value of δ/H suppresses the cellular variation of St along the height for small aspect ratios (Sakamoto and Oiwake, 1984). This range of jet-to-cross-flow velocity ratio, $R < 0.7$, coincides with the downwash flow regime identified by Huang and Hsieh (2002, 2003).

For $R = 0.7$ and 1 (Fig. 6), the magnitude of the Strouhal number is greater than for $R = 0$, 0.5, and 0.6, but remains constant along the stack height. There continues to be no cellular variation of the Strouhal number along the stack height or reduction in the Strouhal number near the free end of the stack. For these values of R, however, the Strouhal number is now measured above the end of the stack (i.e., for $z/H > 1$). This range of jet-to-cross-flow velocity ratio, $0.7 \leqslant R < 1.5$, coincides with the cross-wind-dominated flow regime identified by Huang and Hsieh (2002, 2003).

For $R \geqslant 1.5$ (Fig. 6), there is another change in the behaviour of the Strouhal number. A cellular structure is now observed, with a discontinuity or 'jump' in the Strouhal number along the height of the stack within the stack wake to give two cells of Strouhal number. Moving away from the ground plane, the 'jump' from a lower to higher Strouhal number (e.g., from St = 0.176–0.193 for $R = 2$) occurs inside the flat-plate boundary layer, between $z/H = 0.2$ and 0.5 depending on the value of R. This observed jump in the Strouhal number may be due to the presence of a longitudinal vortex in the uniform flow (Maull and Young, 1973), the change in velocity gradient within and outside the boundary layer thickness, as well as the reduced influence of downwash (with increasing R) on the separated shear layers from the stack. For each particular value of R, the Strouhal number is relatively constant for each cell. The higher Strouhal number value is measured along most of the stack height outside the boundary layer and into the jet wake. Its value is similar to that reported by Eiff and Keffer (1999) for a stack of AR = 8 (see Table 1). For $R = 1.5$, the higher value of the Strouhal number is slightly reduced in magnitude than for $R = 2$–3, whereas the Strouhal number data for $R = 2$ and 2.5 overlap one another (Fig. 6). It is noted that $R = 1.5$ coincides with the transitional flow regime and $R = 2$–3 coincide with the transitional and jet-dominated flow regimes identified by Huang and Hsieh (2002, 2003).

For a finite cylinder, a two-cell structure would be expected for AR = 7–12 for a thin plane wall boundary layer (Lee, 1997). In a uniform flow, Maull and Young (1973) observed a similar cellular structure in the wake of an infinite semi-elliptic nose bluff body, but the higher Strouhal number was at the base region of the bluff body, unlike in the present study. However, for the same model immersed in a shear flow, Maull and Young (1973) found a different cellular

structure, with the lower Strouhal number cells occurring closer to the ground plane, similar to the result of this present work. For a circular cylinder of AR = 8, two cells of different Strouhal number were observed by Mair and Stansby (1975) with the lower portion closer to the base of the cylinder similar to the observation of this present study. Fox and Apelt (1993) made a similar observation for finite cylinders of AR < 13, subjected to a uniform flow.

The presence of a Strouhal number above the stack's free end (i.e., for $z/H > 1$) indicates that vortex shedding activity is also occurring in the jet wake. Since the value of the Strouhal number within the stack and jet wakes is the same (for a particular value of R), it suggests that similar vortices are being shed in both wakes. This result is in agreement with Moussa et al. (1977), who reported that when vortex shedding occurs from the jet, it is controlled by Kármán vortex shedding from the sides of the stack. It is also in agreement with the studies of Eiff et al. (1995) and Eiff and Keffer (1999), who reported "lock-in" of the vortex structures between the stack and jet wakes when $0.63 < d/D < 0.83$; the diameter ratio in the present study is $d/D = 0.67$, which falls within this range.

4.3. Power spectra

Examining the individual power spectra of the streamwise velocity fluctuations, at $R = 0$ (Fig. 7(a)), when there is no jet exiting the stack, considerable variation in the shape and strength of the vortex shedding peak along the height of the stack is observed. The behaviour of the vortex shedding peak at $R = 0$ is similar to the finite-cylinder behaviour observed by Okamoto and Yagita (1973), Okamoto and Sunabashiri (1992), and Sumner et al. (2004). Near the base of the stack and within the flat-plate boundary layer, from $z/H = 0.05$ to about $z/H = 0.25$, weak and broad-banded peaks are observed, indicating a weak but still dominant vortex shedding frequency. Within the mid-height of the stack, from about $z/H = 0.5$ to 0.75, the vortex shedding frequency peak becomes stronger and sharper, indicating stronger and more dominant vortex shedding behaviour. However, at about $z/H = 0.85$–0.95, near the free end of the stack, weaker and more broad-banded peaks become evident. At the free end of the stack, the absence of a prominent peak shows that vortex shedding can no longer be detected. Similar behaviour is observed for $R = 0.5$ (Fig. 7(b)), within the downwash flow regime, but a stronger vortex shedding peak is now found over a larger range of stack height including the top of the stack ($z/H = 1$). The results in Fig. 7(b) show that the presence of the stack jet intensifies vortex shedding from a finite cylinder and makes it more uniform along the cylinder height.

The power spectra for $R = 1$ (Fig. 7(c)) are representative of the cross-wind-dominated flow regime, where the behaviour of the power spectra is similar to that of $R = 0.5$, but the peak occurs at a slightly higher Strouhal number. A weak vortex shedding peak can be identified above the end of the stack (it is still discernible at $z/H = 1.2$; see Fig. 7(c)).

For $R = 1.5$ (Fig. 7(d)), the power spectra close to the base of the stack ($z/H = 0.05$–0.15) have a short broad-banded peak. Moving further from the base, but still within the flat-plate boundary layer, the 'jump' phenomenon noticed in the Strouhal number data in Fig. 6 is seen instead as a gradual change in dominance between two closely spaced peaks (shown more clearly in the inset in Fig. 7(e) for $R = 2.0$) which is similar to the observation of Maull and Young (1973). The dual peaks are seen in the power spectra for $z/H \approx 0.2$–0.5. In the middle of the stack height and outside the flat-plate boundary layer, $z/H = 0.5$–0.85 (Fig. 7(d)), a strong, sharp vortex shedding peak is observed, signifying that strong vortex shedding occurs in this region. Above the free end of the stack and into the jet wake region, $z/H = 1$–1.5, the vortex shedding peak continues to be observed, but the peak strength is much lower.

For $R = 2$–3 (Fig. 7(e,f)), the behaviour of the power spectra is similar to the case of $R = 1.5$, with the double-peak behaviour within the flat-plate boundary layer, and detection of a weakened vortex shedding signal in the jet wake region above the free end of the stack.

A close-up of the double-peak behaviour is shown in the inset in Fig. 7(e). It is seen that the two peaks are very close together, with a sharp high-frequency peak and a wider low-frequency peak being observed. The lower-frequency peak is more prominent closer to the ground plane while the higher-frequency peak becomes dominant further from the ground plane and along the rest of the stack height.

5. Turbulent wake

5.1. Mean velocity field

Mean streamwise velocity profiles ($\bar{U}/U_\infty$) on the wake centreline ($y/D = 0$), at $x/D = 10$, are shown in Fig. 8(a) for several jet-to-cross-flow velocity ratios. Three distinct flow regimes can be roughly identified, which are: downwash flow, cross-wind-dominated flow and jet-dominated flow. Generally, the size of the stack wake decreases with R while the size of the jet wake increases with R. For $R < 2$, the bent-over jet is not noticeable at $x/D = 10$ since the mean velocity remains lower than the freestream velocity ($\bar{U}/U_\infty \leqslant 1$) in the combined stack wake and jet wake.

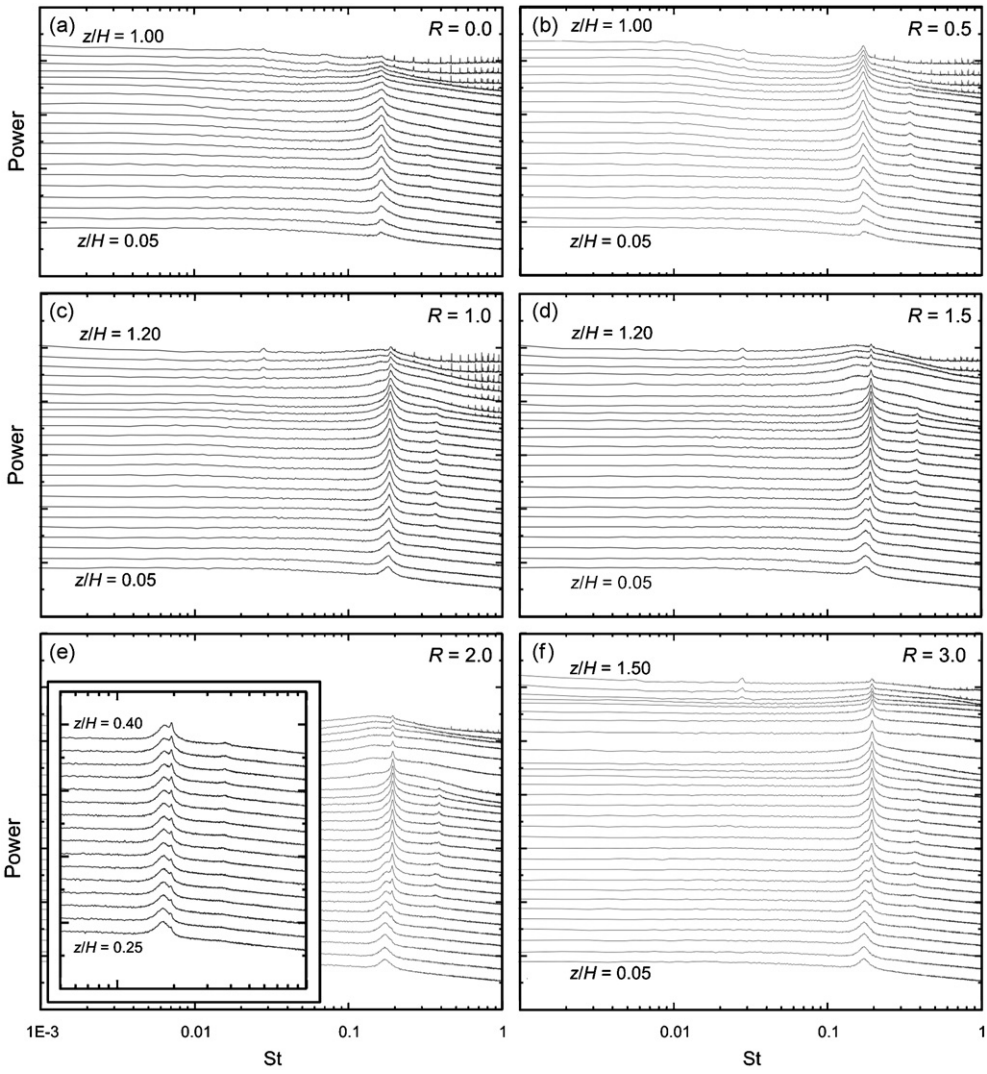

Fig. 7. Power spectra along the height of the stack, measured at $x/D = 3$ and $y/D = 1.5$, starting at $z/H = 0.05$, at an interval of $\Delta z/H = 0.05$: (a) $R = 0$; (b) $R = 0.5$; (c) $R = 1$; (d) $R = 1.5$; (e) $R = 2$, with inset showing spectra at an interval of $\Delta z/H = 0.01$; (f) $R = 3$. Each spectrum represents 250 averages. The vertical logarithmic scale is arbitrary, but the same scale is used for each spectrum throughout the figure.

When $R = 0$, the large velocity defect shows that only the stack wake is observed. When $R = 0.5$, the velocity profile is almost similar to that of $R = 0$, but there is second, smaller velocity defect within the stack wake below the stack free end. The flow regime that falls within $R \leqslant 0.5$ is termed downwash flow, which is similar to the downwash flow regime identified by Huang and Hsieh (2002, 2003).

For $R = 1$, the mean velocity profile is distinct from those for $R = 0$ and 0.5. The main velocity defect in the stack wake is reduced, while the second region of velocity defect is greater in size and magnitude and is shifted upwards towards the free end of stack. The unique shape of this mean profile indicates a change from the downwash to the cross-wind-dominated flow regime.

At $R = 1.5$, the bent jet behaves completely as another bluff body and produces a jet wake in addition to the stack wake. This is indicated by the presence of a velocity defect region above the stack's free end. This is in agreement with Onbaşioğlu (2001) who noted that a discharged jet into a cross-flow behaves similarly to an obstacle placed in the flow. As the value of R increases, the vertical extent of the jet wake also increases, which shows that the jet rise increases with R. When $R \geqslant 2$, in addition to the wake features, there is another region in the profile corresponding to the stack jet

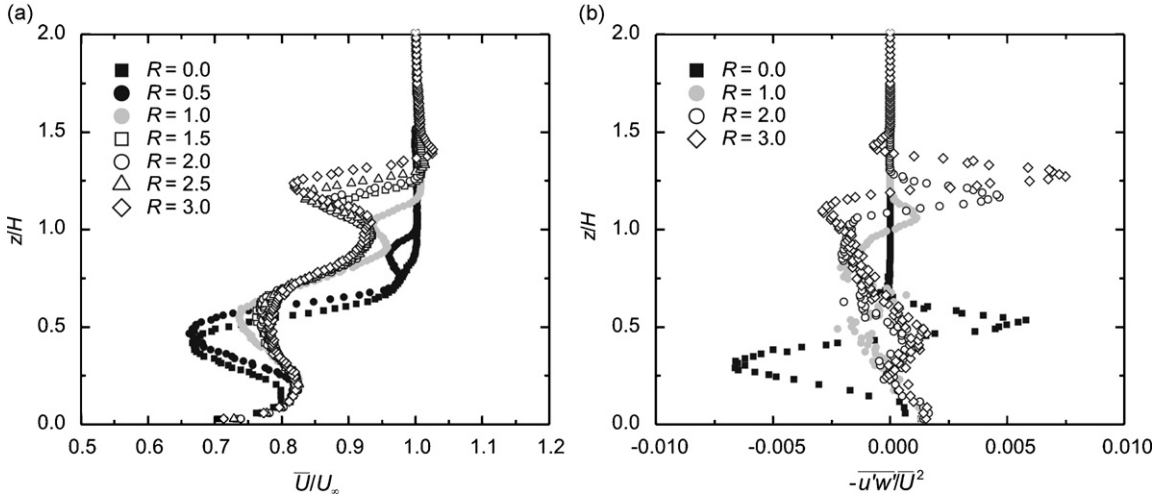

Fig. 8. Measurements on the wake centreline ($y/D = 0$) at $x/D = 10$: (a) mean streamwise velocity; (b) Reynolds shear stress.

where the local streamwise velocity is greater than the freestream velocity due to the presence of the jet flow. This range of R broadly corresponds to the transitional and jet-dominated flow regimes proposed by Huang and Hsieh (2002, 2003).

Either the location of the maximum streamwise velocity or the maximum value of the in-plane velocity magnitude, $(\bar{U}^2 + \bar{W}^2)^{0.5}$, can be used to determine the location of the jet centreline. Based on both approaches, the jet centrelines at $x/D = 10$ are located at $z/H = 1.31$, 1.34, 1.41 and 1.47 for $R = 1.5$, 2, 2.5, and 3, respectively, above the ground plane. This clearly shows that the jet rise increases with R due to the increased penetration strength of the jet.

The time-averaged streamwise velocity fields ($\bar{U}/U_\infty$) in the cross-stream (y–z) plane at $x/D = 10$ are shown as contour plots in Fig. 9 for different jet-to-cross-flow velocity ratios. As R increases, the lateral spread of the stack wake decreases and the maximum velocity defect reduces. Similar reductions are observed for a finite circular cylinder when its aspect ratio is increased (Adaramola et al., 2006). In the downwash flow regime, a region of low mean streamwise velocity is observed behind and within the wake of the stack and well above the ground plane (for $R = 0$, Fig. 9(a)) and a second low velocity region begins to form near the top of the stack but within the stack wake (when $R = 0.5$, Fig. 9(b)). In the cross-wind-dominated flow regime, this second region forms just above the stack free end (when $R = 1$, Fig. 9(c)). In the case of the jet-dominated flow regime (when $R = 1.5$, Fig. 9(d); $R = 2$, Fig. 9(e); $R = 2.5$, Fig. 9(f); $R = 3$, Fig. 9(g)), the second region occurs above the free end of the stack, is better defined and more isolated from the stack wake, and clearly represents the jet wake. As R increases, this region moves further above the free end of the stack and the extent of the region expands. This shows that the jet wake size increases and the jet rise increases.

The wall-normal mean velocity ($\bar{W}/U_\infty$) fields in the cross-stream plane at $x/D = 10$ are shown in Fig. 10. The presence of a strong downwash flow (represented by the dashed contour lines, and indicating a region of downward-directed velocity originating from the free end of the stack) is observed for nearly all values of R except for the highest velocity ratios tested in the jet-dominated flow regime. The position of the downwash flow region above the ground plane increases with R due to the strengthening of the jet. In the downwash flow regime, the downwash flow associated with the weak jet is almost completely inside the stack wake (Fig. 10(a,b)). In the case of the cross-wind-dominated flow regime (Fig. 10(c)), the strength of the downwash flow reduces due to the increase in the penetrating power of the jet. In the jet-dominated flow (Fig. 10(d–g)), the downwash flow weakens further and by $R = 2.5$ (Fig. 10(f)) it is entirely absent. The strength of the downwash flow reduces with increasing R, with a maximum downwash magnitude of $\bar{W}/U_\infty = -0.16$, -0.14, -0.10, -0.06, and -0.05 for $R = 0$, 0.5, 1, 1.5, and 2, respectively.

Closer to the base of the stack, upwash flow from the ground plane and within the wake of the stack and the ground plane boundary layer region is observed for all values of R. The strength of this upwash flow seems to be relatively independent of the value of R but stretches upward toward the free end of the stack as the value of R increases. When $R = 2$ (Fig. 10(e)), another upwash flow region begins to develop within the jet wake and above the stack free end, which is characteristic of the jet-dominated flow regime. The size and strength, as well as the vertical position, of this upwash region in the jet wake increase with R.

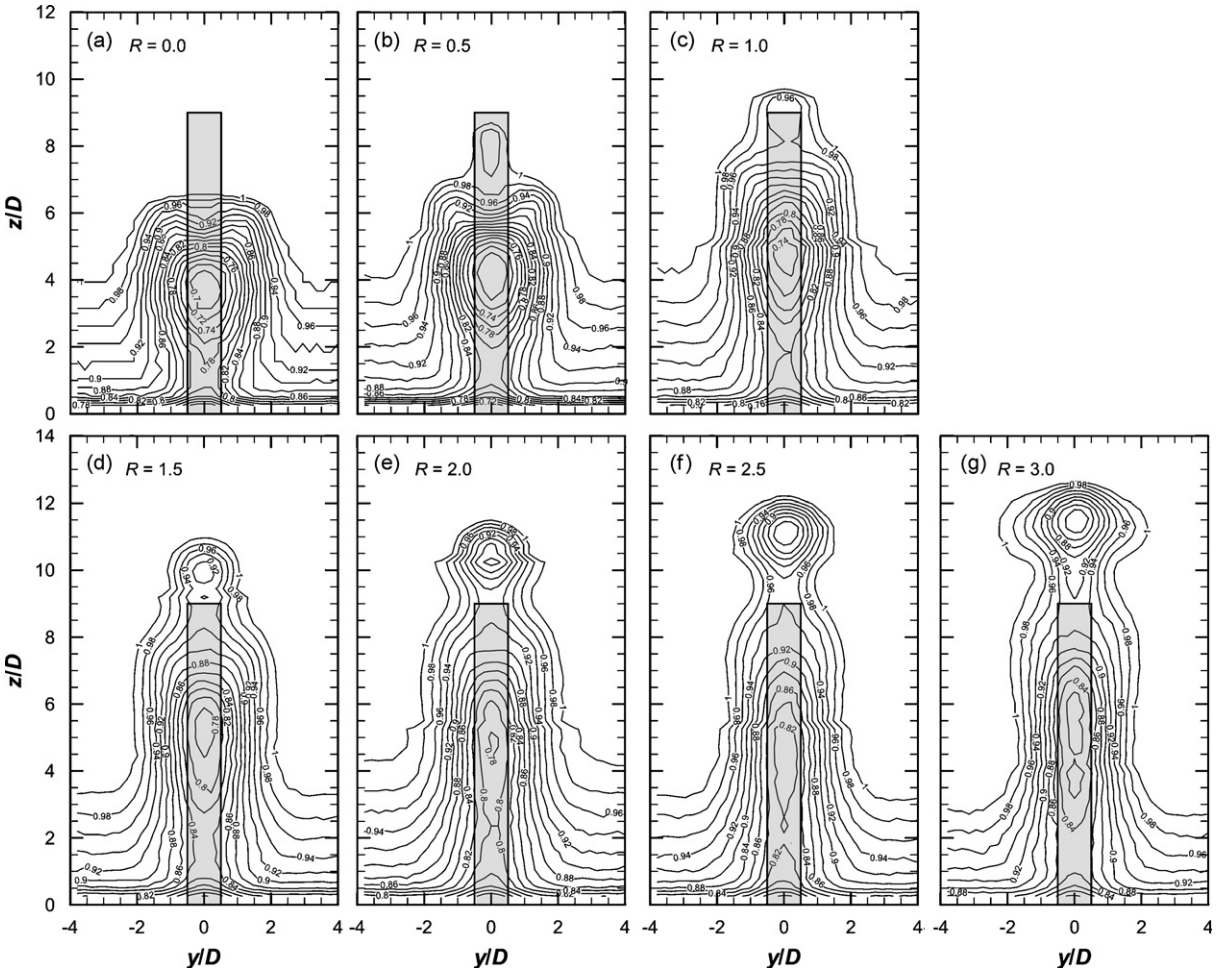

Fig. 9. Streamwise mean velocity field in the wake of the stack, $x/D = 10$: (a) $R = 0$; (b) $R = 0.5$; (c) $R = 1$; (d) $R = 1.5$; (e) $R = 2$; (f) $R = 2.5$; (g) $R = 3$. Contours of $\bar{U}/U_\infty$, minimum contour 0.02, contour increment of 0.02.

5.2. Turbulence intensities

Fig. 11 shows the streamwise turbulence intensity ($u'/\bar{U}$) fields in the cross-stream plane at $x/D = 10$. Localized regions of high streamwise turbulence intensity in the stack and jet wakes (Fig. 11) coincide with the regions of low streamwise mean velocity (Fig. 9). For the finite circular cylinder ($R = 0$, Fig. 11(a)), the high turbulence intensity behind the stack is attributed to the interactions between the streamwise vortex structures, the vortex street, downwash from the free end, and upwash from the ground plane, which produces strong shear (Sumner et al., 2004; Adaramola et al., 2006). In the downwash flow regime, when $R = 0.5$ (Fig. 11(b)), a second region of high turbulence intensity begins to form near the top of the stack and within the stack wake. In the cross-wind-dominated flow regime ($R = 1$, Fig. 11(c)), this second region extends above the free end of the stack. In the jet-dominated flow regime, for $R = 1.5$–3 (Fig. 11(d–g)) this second region of elevated streamwise turbulence intensity becomes more distinct, increases in size, and moves further above the free end of the stack, characterizing the jet wake region. The behaviour of the second region of high turbulence intensity demonstrates the influence of the jet flow, which is relatively weak when $R < 1.5$ but becomes increasingly stronger when $R \geqslant 1.5$. The high turbulence intensities within the jet wake can be attributed to the strong mixing (which increases with R) between the jet flow and cross-flow, especially in the cross-wind-dominated and jet-dominated flow regimes.

The wall-normal turbulence intensity data ($w'/\bar{U}$), shown in Fig. 12, behave similarly to the streamwise turbulence intensity data for all values of R. In contrast to Huang and Hsieh (2002, 2003), it was observed that both the streamwise and wall-normal turbulence intensities were generally greater in the stack wake than in the jet wake.

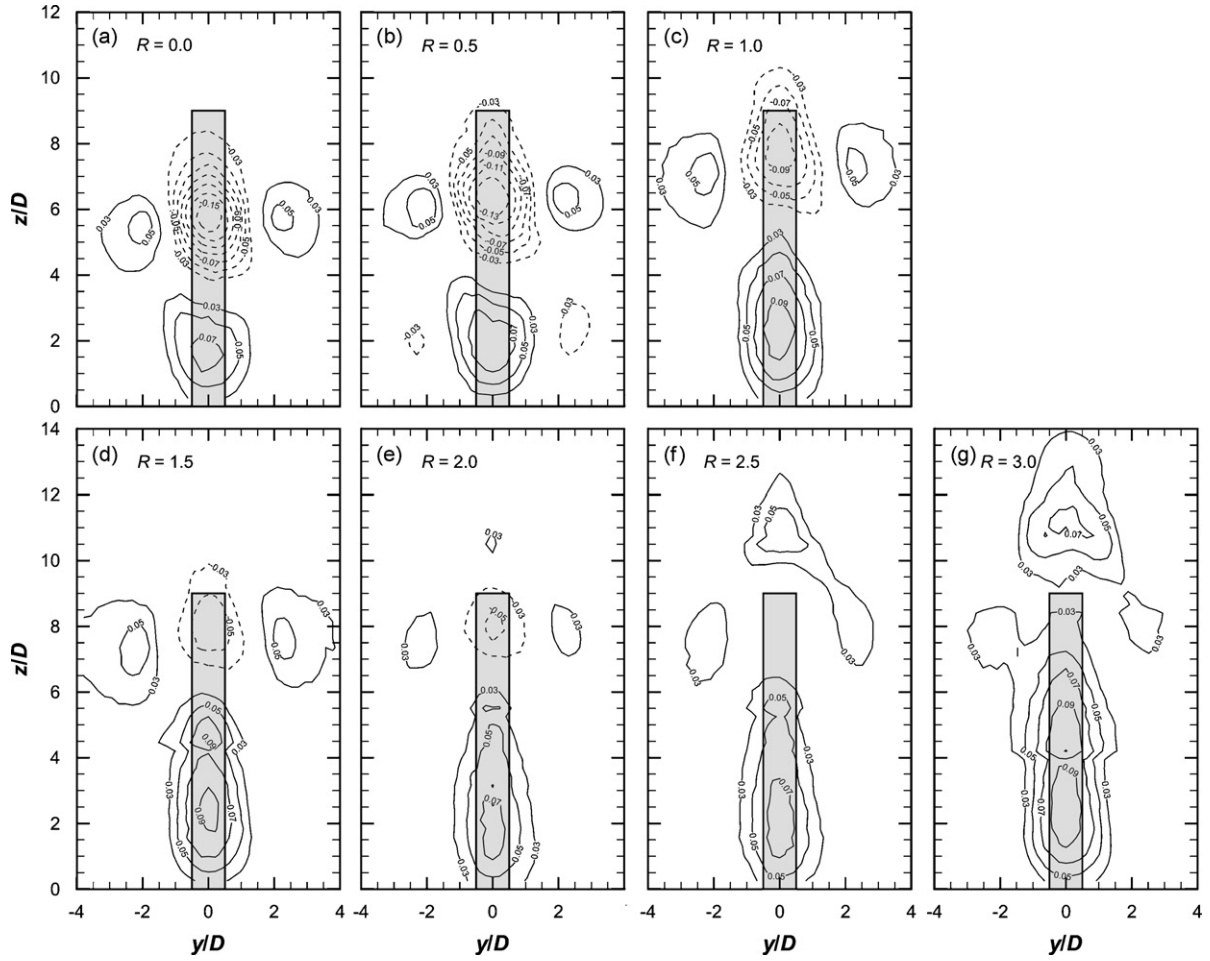

Fig. 10. Wall-normal mean velocity field in the wake of the stack, $x/D = 10$: (a) $R = 0$; (b) $R = 0.5$; (c) $R = 1$; (d) $R = 1.5$; (e) $R = 2$; (f) $R = 2.5$; (g) $R = 3$. Contours of $\bar{W}/U_\infty$, minimum contour magnitude 0.03, contour increment of 0.02, solid contour lines represent positive wall-normal velocity, dashed contour lines represent negative wall-normal velocity.

5.3. Reynolds shear stress

Reynolds shear stress ($-\overline{u'w'}\Big/\bar{U}^2$) profiles on the wake centreline ($y/D = 0$) at $x/D = 10$ are shown in Fig. 8(b). Physically, the Reynolds shear stress relates to the transport of momentum due to the turbulent fluctuations in the flow. Regions of elevated Reynolds shear stress may be associated with either strong positive or negative production of turbulence, depending on the local velocity gradients.

In the downwash flow regime ($R \leqslant 0.5$), there are two regions of elevated Reynolds shear stress, each of opposite sign, located behind the stack (Fig. 8(b)), similar to what was reported by Adaramola et al. (2006) for a finite circular cylinder. The region of positive Reynolds shear stress coincides with the downwash flow from the free end (see Fig. 10(a,b)). The region of negative Reynolds shear stress, within the flat-plate boundary layer, coincides with the upwash flow from the ground plane (see Fig. 10(a,b)). The boundary between these two regions, where the Reynolds shear stress is zero, approximately coincides with the region of lowest streamwise mean velocity (see Fig. 9(a,b)) and highest turbulence intensity (Figs. 11(a,b) and 12(a,b)).

For the cross-wind-dominated flow regime ($R = 1$), there is a reduction in the magnitude of the Reynolds stress compared to the downwash flow regime and the finite circular cylinder (Fig. 8(b)). In addition, the Reynolds stress in the stack wake becomes entirely negative; there is only a small region of positive Reynolds stress, which occurs in the jet wake just above the stack's free end (Fig. 8(b)).

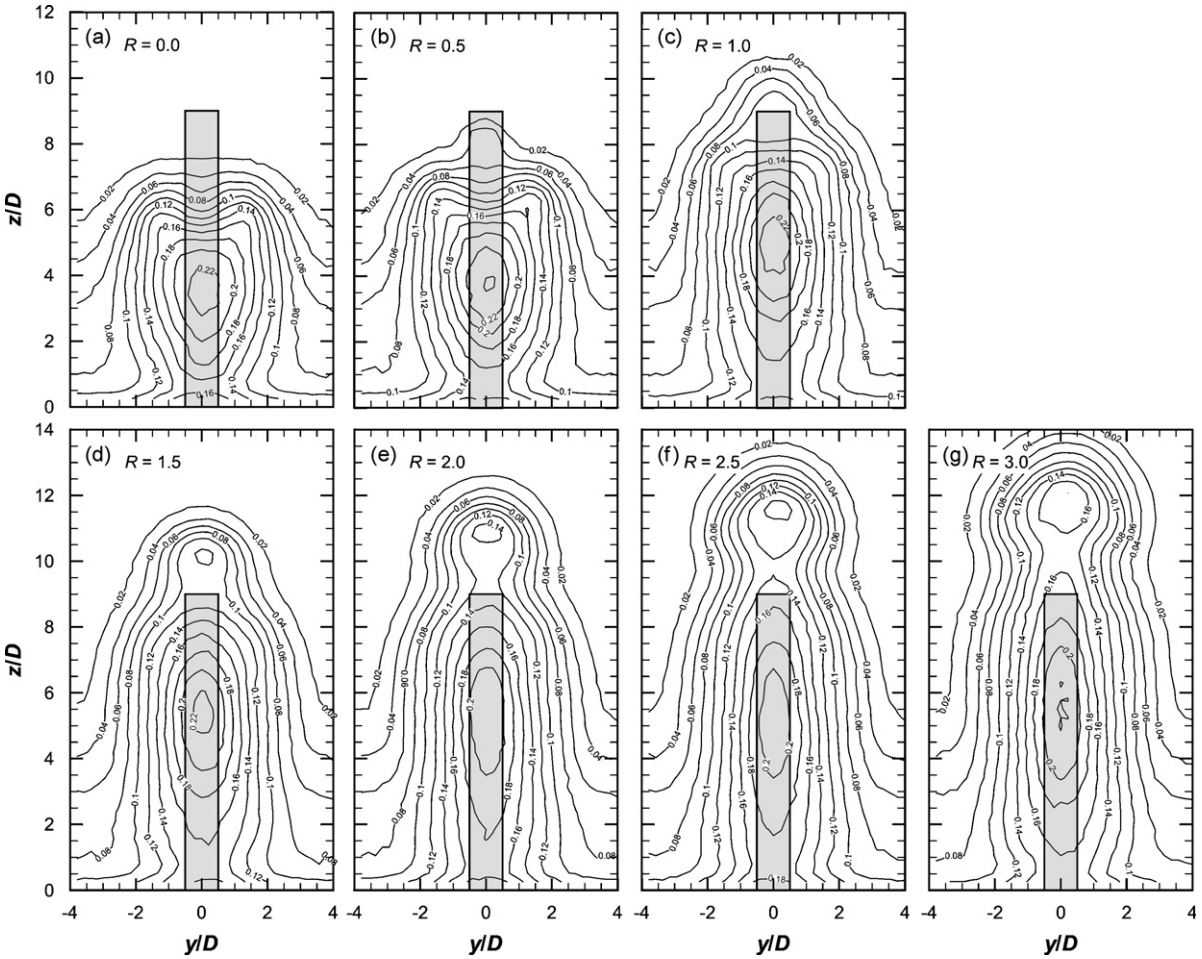

Fig. 11. Streamwise turbulence intensity field in the wake of the stack, $x/D = 10$: (a) $R = 0$; (b) $R = 0.5$; (c) $R = 1$; (d) $R = 1.5$; (e) $R = 2$; (f) $R = 2.5$; (g) $R = 3$. Contours of $u'/\bar{U}$, minimum contour 0.02, contour increment of 0.02.

In the jet-dominated flow regime ($R = 2$ and 3), the stack wake remains a region of negative Reynolds stress. The positive Reynolds shear stress within the jet wake is now more prominent and attains a higher strength compared to the cross-wind-dominated flow regime (Fig. 8(b)).

The contour plots for the Reynolds stress behind the stack at $x/D = 10$ are presented in Fig. 13. In the downwash flow regime ($R = 0$ and 0.5, Fig. 13(a,b)), there is a concentrated region of negative Reynolds shear stress in the lower part of the stack wake within the flat-plate boundary layer. It is in this region, where the upwash velocity is found (Fig. 10(a,b)), that the base vortex structures are located (Sumner et al., 2004), and the Kármán vortex axes have been observed to bend upstream toward the base of the stack (Okamoto and Yagita, 1973; Johnston and Wilson, 1997; Tanaka and Murata, 1999). There are also two regions of negative Reynolds stress on either side of the stack closer to the free end. This pair may be due to several aspects of the flow field, including the upwash flow on the outer edges of the stack wake (see Fig. 10(a,b)), the tip vortex structures (Sumner et al., 2004), and the bending of Kármán vortex axes toward the free end (Okamoto and Yagita, 1973; Johnston and Wilson, 1997; Tanaka and Murata, 1999). The strength of this pair is lower than that of the concentrated region inside the flat-plate boundary layer because the upwash flow from the ground plane is stronger than the upwash flow in the upper half of the stack wake. The pair moves closer to the free end when jet flow occurs (compare $R = 0$ with $R = 0.5$, Fig. 13(a,b)). In between these regions of negative Reynolds shear stress, at the edge of the flat-plate boundary layer, is a small region of concentrated positive Reynolds stress. The absolute strength of this positive region is lower than that of the negative region, but is higher for $R = 0.5$ than for $R = 0$.

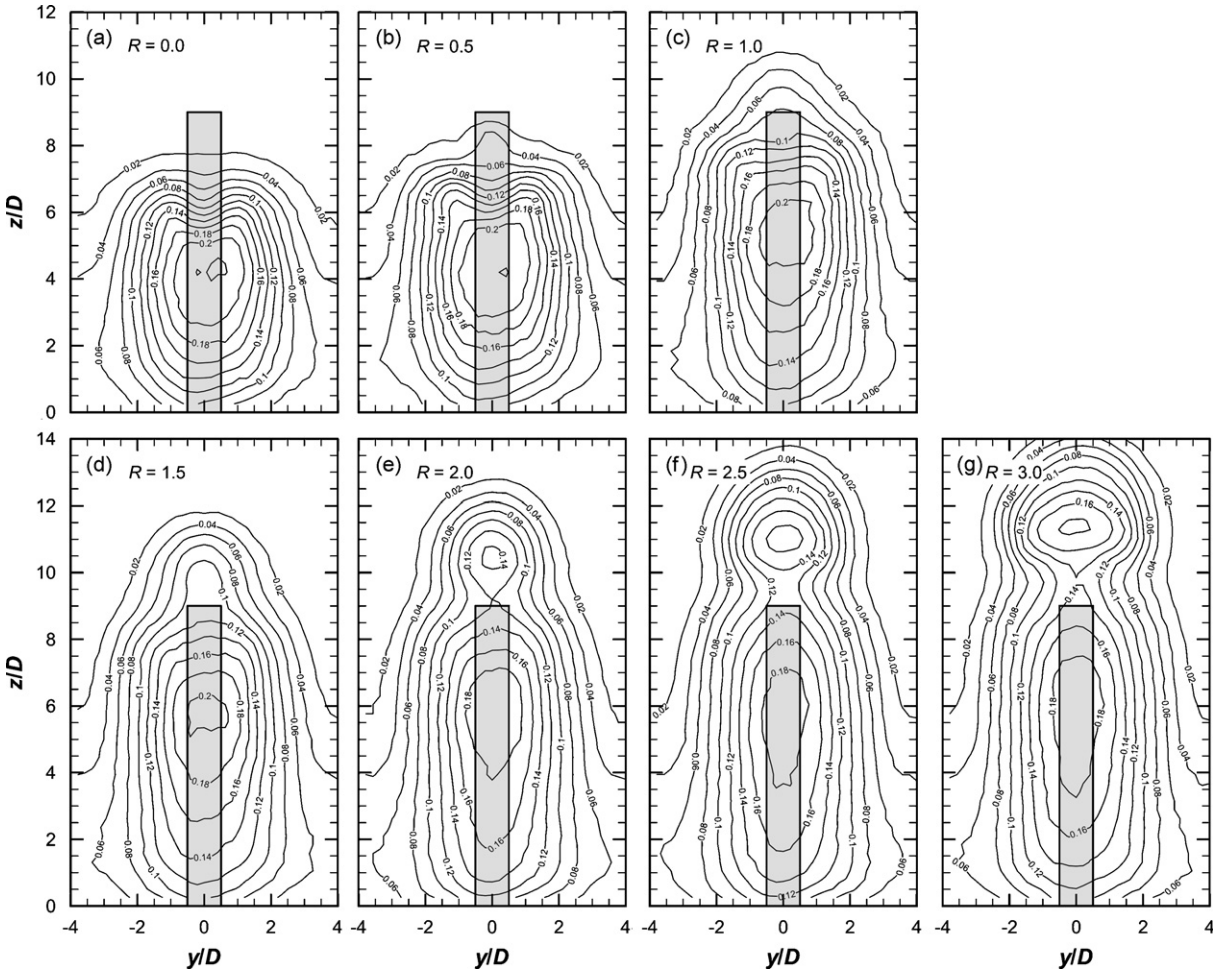

Fig. 12. Wall-normal turbulence intensity field in the wake of the stack, $x/D = 10$: (a) $R = 0$; (b) $R = 0.5$; (c) $R = 1$; (d) $R = 1.5$; (e) $R = 2$; (f) $R = 2.5$; (g) $R = 3$. Contours of $w'/\bar{U}$, minimum contour 0.02, contour increment of 0.02.

In the cross-wind-dominated flow regime ($R = 1$, Fig. 13(c)), the Reynolds stress in the stack wake has weakened considerably and is now entirely negative. This is also seen in throughout the stack wake in the jet-dominated flow regime ($R = 1.5$–3, Fig. 13(d–g)).

Elsewhere in the jet-dominated flow regime, a small region of positive Reynolds shear stress is observed above the stack free end and within the jet wake; it coincides with a region of low mean streamwise velocity that occurs within the jet wake (Fig. 9(d–g)). As R increases and the jet rises further, the size, strength, and vertical position of this region of positive Reynolds shear stress increase, while the region of negative Reynolds shear stress extends upward above the stack's free end (Fig. 13(d–g)). This strong Reynolds shear stress field in the jet wake indicates the product.

6. Conclusions

In the present study, thermal anemometry was used to measure the turbulent wake and vortex shedding frequency for a small-aspect-ratio (AR = 9) cylindrical stack partially immersed in a flat-plate turbulent boundary layer $\delta/H = 0.5$). A single-sensor hot-wire was used to measure the vortex shedding frequency along the stack height and into the jet wake region. A two-component X-probe was used to measure the turbulent velocity field both in a vertical (x–z) plane along the wake centreline but also in the cross-stream (y–z) plane. The latter wake measurements, in the cross-stream (y–z) plane, complement and extend the results presented in earlier studies of this flow, by Eiff et al. (1995), Eiff and Keffer (1997, 1999), and Huang and Hsieh (2002, 2003).

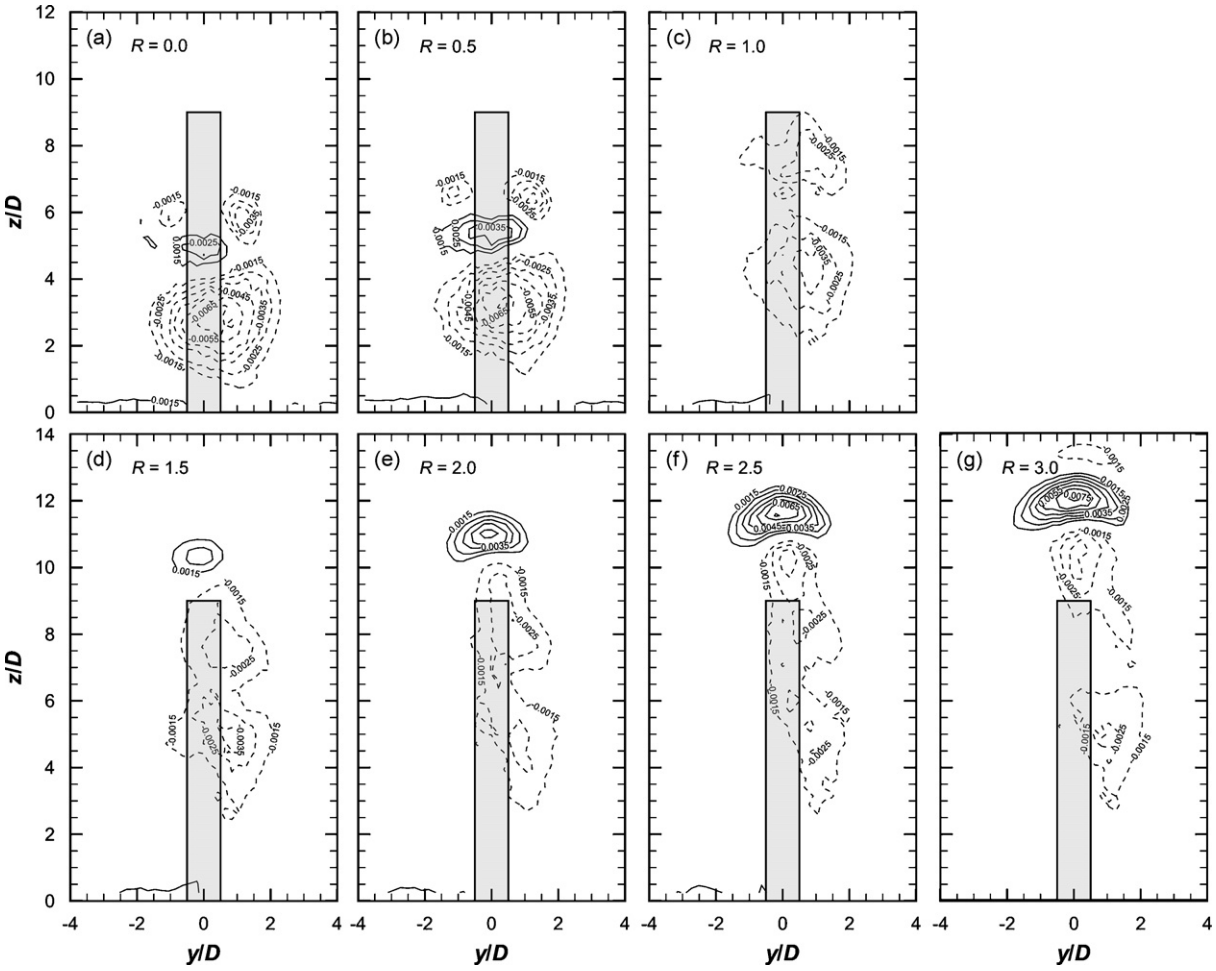

Fig. 13. Reynolds shear stress field in the wake of the stack, $x/D = 10$: (a) $R = 0$; (b) $R = 0.5$; (c) $R = 1$; (d) $R = 1.5$; (e) $R = 2$; (f) $R = 2.5$; (g) $R = 3$. Contours of $-\overline{u'w'}/\bar{U}^2$, minimum contour magnitude 0.0015, contour increment of 0.0015, solid contour lines represent positive Reynolds shear stress, dashed contour lines represent negative Reynolds shear stress.

By varying the jet-to-cross-flow velocity ratio, R, and observing the resulting changes in the mean velocity field, turbulence intensity field, Reynolds stress field, and the Strouhal number, the near-field behaviour of the stack and jet wake regions could be broadly classified into three flow regimes. These were classified as the downwash flow regime ($R < 0.7$), cross-wind-dominated flow regime ($0.7 \leqslant R < 1.5$), and jet-dominated flow regime ($R \geqslant 1.5$), adopting the terminology used by Huang and Hsieh (2002, 2003). From the measurements made in the present study, it was not possible to clearly discern a transitional flow regime, as identified by Huang and Hsieh (2002, 2003); this may be partially due to the limited number of jet-to-cross-flow velocity ratios considered in the present study.

From the single-sensor hot-wire measurements, the behaviour of the vortex formation length and the vortex shedding frequencies (Strouhal numbers) were examined. At the mid-height of the stack ($z/H = 0.5$), the vortex formation length decreases with increasing R, indicating the stack wake becomes more two-dimensional and similar to that observed behind an infinite (or higher-aspect-ratio) circular cylinder. This change in the local flow field was supported by the Strouhal number measurements, which showed the Strouhal number for the stack approaches the value for an infinite circular cylinder with an increase in R. In the downwash flow regime, a Strouhal number of $\mathrm{St} = 0.166$ was measured, which was independent of the position along the height of the stack. In the cross-wind-dominated flow regime, a higher Strouhal number of $\mathrm{St} = 0.186$ was measured. In the jet-dominated flow regime, when $R \geqslant 1.5$, a different Strouhal number behaviour was observed, with a 'jump' in Strouhal number from $\mathrm{St} = 0.176$ to 0.193 occurring within the flat-plate turbulent boundary layer. The higher value of $\mathrm{St} = 0.193$, which is close to the value for an infinite circular cylinder, continued to be measured in the jet-wake region. This was evidence of the "lock-in" of the Kármán-type

vortex structures between the stack and jet wakes, and showed that the higher-momentum jet acts in a similar manner to a bluff body, effectively extending the stack's aspect ratio and allowing the Kármán-type vortex structures to extend above the stack's free end.

From the two-component thermal anemometry measurements of the stack wake and jet wake regions, marked changes in the flow pattern were observed as R was increased from 0 to 3, and as the flow regime changed from downwash to cross-wind-dominated and then to jet-dominated. Each flow regime has a distinct structure for the mean velocity (streamwise and wall-normal components), turbulence intensity (streamwise and wall-normal components), and Reynolds shear stress fields.

For the mean velocity field, the strength of the downwash velocity decreases as R increases, and the upwash velocity field extends further above the ground plane. In the jet-dominated flow regime, there is an absence of appreciable downwash flow. There are two main regions of low streamwise mean velocity, one located behind the stack and one located in the jet wake region.

For the turbulence structure, complex changes occur in the streamwise and wall-normal directions within the near and intermediate stack and jet wakes. In general, the streamwise and wall-normal turbulence intensity fields are characterized by two regions of elevated turbulence, that coincide with regions of low streamwise mean velocity in the stack and jet wakes. In the downwash flow regime, high levels of turbulence intensity are found in the stack wake region. In the cross-wind-dominated flow regime, the second region of high turbulence intensity occurs just above the free end of the stack. In the jet-dominated flow regime, this second region occurs entirely within the jet-wake. The Reynolds shear stress field also undergoes marked changes with an increase in R. In the downwash flow regime, the lower stack wake is a region of negative Reynolds stress and the upper stack wake is a region of positive Reynolds stress. In cross-wind-dominated flow regime, the region of negative Reynolds stress weakens but extends farther away from the ground plane throughout the stack wake. In the jet-dominated flow regime, a region of strong positive Reynolds stress forms within the jet wake.

Acknowledgements

The authors acknowledge the financial support of the Natural Sciences and Engineering Research Council (NSERC) of Canada, the Canada Foundation for Innovation (CFI), the Innovation and Science Fund of Saskatchewan, and the Division of Environmental Engineering. The assistance of D.M. Deutscher, A.O. Oladeinde, and Engineering Shops is appreciated.

References

Adaramola, M.S., Akinlade, O.J., Sumner, D., Bergstrom, D.J., Schenstead, A.J., 2006. Turbulent wake of a finite circular cylinder of small aspect ratio. Journal of Fluids and Structures 22, 919–928.

Andreopoulos, J., Rodi, W., 1984. Experimental investigation of jets in a crossflow. Journal of Fluid Mechanics 138, 93–127.

Arya, S.P.S., Lape, J.F., 1990. A comparative study of the different criteria for the physical modeling of buoyant plume rise in a neutral atmosphere. Atmospheric Environment 24A, 289–295.

ASHRAE, 1999. Handbook of HVAC Operations: Building Air Intake and Exhaust Design. ASHRAE, Atlanta, USA (Chapter 43).

ASHRAE, 2001. Handbook of Fundamentals: Airflow Around Buildings. ASHRAE, Atlanta, USA (Chapter 16).

Briggs, G.A., 1984. Plume rise and buoyancy effects. Atmospheric Science and Power Production. Office of Scientific and Technical Information Centre, USDOE, DOE/TIC-27601 (DE 84005177), pp. 327–366.

Eiff, O.S., Keffer, J.F., 1997. On the structures in the near wake region of an elevated turbulent jet in a crossflow. Journal of Fluid Mechanics 333, 161–195.

Eiff, O.S., Keffer, J.F., 1999. Parametric investigation of the wake-vortex lock-in for the turbulent jet discharging from a stack. Experimental Thermal and Fluid Science 19, 57–66.

Eiff, O.S., Kawall, J.G., Keffer, J.F., 1995. Lock-in of vortices in the wake of an elevated round turbulent jet in a crossflow. Experiments in Fluids 19, 203–213.

Etzold, F., Fiedler, H., 1976. The near-wake structure of a cantilevered circular cylinder in a cross-flow. Zeitschrift fuer Flugwissenschaften 24, 77–82.

Farivar, D.J., 1981. Turbulent uniform flow around cylinders of finite length. AIAA Journal 19, 275–281.

Fox, T.A., Apelt, C.J., 1993. Fluid-induced loading on cantilevered circular cylinders in a low-turbulence uniform flow. Part 3: Fluctuating loads with aspect ratios 4–25. Journal of Fluids and Structures 7, 375–386.

Fric, T.F., Roshko, A., 1994. Vortical structure in the wake of a transverse jet. Journal of Fluid Mechanics 279, 1–47.

Griffin, O.M., 1985. Vortex shedding from bluff bodies in a shear flow: a review. ASME Journal of Fluids Engineering 107, 298–306.

Hsieh, R.H., Huang, R.F., 2003. Tomographic flow structures of a round jet in a crossflow. Journal of the Chinese Institute of Engineers 26, 71–80.

Huang, R.F., Hsieh, R.H., 2002. An experimental study of elevated round jets deflected in a crossflow. Experimental Thermal and Fluid Science 27, 77–86.

Huang, R.F., Hsieh, R.H., 2003. Sectional flow structures in near wake of elevated jet in a crossflow. AIAA Journal 41, 1490–1499.

Huang, R.F., Lan, J., 2005. Characteristic modes and evolution processes of shear-layer vortices in an elevated transverse jet. Physics of Fluids 17, 034103.

Johnston, C.R., Wilson, D.J., 1997. A vortex pair model for plume downwash into stack wakes. Atmospheric Environment 31, 13–20.

Kawamura, T., Hiwada, M., Habino, T., Mabuchi, I., Kumada, M., 1984. Flow around a finite circular cylinder on a flat plate. Bulletin of the JSME 27, 2142–2150.

Kitagawa, T., Wakahara, T., Fujino, Y., Kimura, K., 1997. An experimental study on vortex-induced vibration of a circular cylinder tower at a high wind speed. Journal of Wind Engineering and Industrial Aerodynamics 69–71, 731–744.

Leder, A., 2003. 3D-flow structures behind truncated circular cylinders. In: Proceedings of FEDSM'03, fourth ASME-JSME Joint Fluids Engineering Conference. Honolulu, USA, Paper No. FEDSM2003-45083.

Lee, L.W., 1997. Wake structure behind a circular cylinder with a free end. In: Proceedings of the Heat Transfer and Fluid Mechanics Institute. pp. 241–251.

Lee, L.W., Wang, Y.L., 1987. Aerodynamics of a circular cylinder of finite length in cross-flow. In: Proceedings of the ASME Applied Mechanics, Bioengineering, and Fluids Engineering Conference. Cincinnati, USA, pp. 61–65.

Mair, W.A., Stansby, P.K., 1975. Vortex wakes of bluff cylinders in shear flow. SIAM Journal on Applied Mathematics 28 (2), 519–540.

Maull, D.J., Young, R.A., 1973. Vortex shedding from bluff bodies in a shear flow. Journal of Fluid Mechanics 60, 401–409.

McMahon, H.M., Hester, D.D., Palfery, J.G., 1971. Vortex shedding from a turbulent jet in a cross-wind. Journal of Fluid Mechanics 48, 73–80.

Moussa, Z.M., Trischka, J.W., Eskinazi, S., 1977. The near field in the mixing of a round jet with a cross-stream. Journal of Fluid Mechanics 80, 49–80.

Noca, F., Park, H.G., Gharib, M., 1998. Vortex formation length of a circular cylinder ($300 < Re < 4{,}000$) using PIV. In: Proceedings of ASME FEDSM'98. ASME, Washington, DC, New York, pp. 46–53.

Norberg, C., 1986. Interaction between freestream turbulence and vortex shedding for a single tube in cross-flow. Journal of Wind Engineering and Industrial Aerodynamics 23, 501–514.

Okamoto, S., Sunabashiri, Y., 1992. Vortex shedding from a circular cylinder of finite length placed on a ground plane. ASME Journal of Fluids Engineering 114, 512–521.

Okamoto, T., Yagita, M., 1973. The experimental investigation on the flow past a circular cylinder of finite length placed normal to the plane surface in a uniform stream. Bulletin of the JSME 16, 805–814.

Onbaşıoğlu, S.U., 2001. On the simulation of the plume from stacks of buildings. Building and Environment 36, 543–559.

Overcamp, T.J., Ku, T., 1988. Plume rise from two or more adjacent stacks. Atmospheric Environment 22, 625–637.

Park, C.-W., Lee, S.-J., 2000. Free end effects on the near wake flow structure behind a finite circular cylinder. Journal of Wind Engineering and Industrial Aerodynamics 88, 231–246.

Park, C.-W., Lee, S.-J., 2004. Effects of free-end corner shape on flow structure around a finite cylinder. Journal of Fluids and Structures 19, 141–158.

Sakamoto, H., Oiwake, S., 1984. Fluctuating forces on a rectangular prism and a circular cylinder placed vertically in a turbulent boundary layer. ASME Journal of Fluids Engineering 106, 160–166.

Schulman, L.L., Scire, J.S., 1991. The effect of stack height, exhaust speed, and wind direction on concentrations from a rooftop stack. ASHRAE Transactions 97, 573–582.

Sumner, D., Heseltine, J.L., Dansereau, O.J.P., 2004. Wake structure of a finite circular cylinder of small aspect ratio. Experiments in Fluids 37, 720–730.

Tanaka, S., Murata, S., 1999. An investigation of the wake structure and aerodynamic characteristics of a finite circular cylinder. JSME International Journal Series B: Fluids and Thermal Engineering 42, 178–187.

Taniguchi, S., Sakamoto, H., Arie, M., 1981. Flow around circular cylinders of finite height placed vertically in turbulent boundary layers. Bulletin of the JSME 24, 37–44.

Uematsu, Y., Yamada, M., Ishii, K., 1990. Some effects of free-stream turbulence on the flow past a cantilevered circular cylinder. Journal of Wind Engineering and Industrial Aerodynamics 33, 43–52.

Wilson, D.J., 1979. Flow patterns over flat-roofed buildings and application to exhaust stack design. ASHRAE Transactions 85, 284–295.